Macromolecules

pubs.acs.org/Macromolecules Article

Mussel-Inspired Copolyether Loop with Superior Antifouling Behavior

Eeseul Shin,[⊥] Chanoong Lim,[⊥] Uk Jung Kang,[⊥] Minseong Kim, Jinwoo Park, Dongseok Kim, Woojin Choi, Jinkee Hong, Chunggi Baig,* Dong Woog Lee,* and Byeong-Su Kim*

Cite This: https://dx.doi.org/10.1021/acs.macromol.0c00481 Read Online

ACCESS | Metrics & More | Article Recommendations | Supporting Information

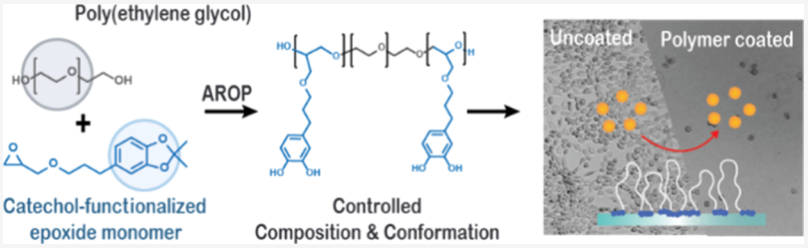

ABSTRACT: Poly(ethylene glycol) (PEG) has attracted significant interest because of its superior antifouling properties, water solubility, and biocompatibility. However, the translation of its antifouling properties onto target surfaces has been challenging because of its limited functionality. Herein, the superior antifouling properties of PEG-based block copolyethers functionalized with catechol, a mussel-inspired, versatile moiety for coating surfaces, were evaluated within a framework of polyethers exclusively. A series of catechol-functionalized polyethers with diverse molecular weights and catechol contents were synthesized via anionic ring-opening polymerization in a controlled manner. The versatile adsorption and antifouling effects of block copolyethers were evaluated using a quartz crystal microbalance with dissipation. Furthermore, the crucial role of the topology (loop vs brush) in the antifouling properties was analyzed via a surface force apparatus and direct atomistic molecular dynamics simulations. This study demonstrates that the catechol-functionalized triblock copolymer shows excellent antifouling properties, exhibiting its great potential in various biomedical applications.

INTRODUCTION

Biofouling, the undesirable accumulation of biomolecules and organisms on wet surfaces, poses significant challenges in a wide range of fields ranging from biomedical implants to industrial and marine equipment.[1,2] While the use of biocides is the most popular means for effectively inhibiting the accumulation of marine organisms, the toxic chemicals or heavy metals present in the biocides can present considerable threats to marine environments. Therefore, improving the antifouling properties of surfaces has become crucial to reducing the chance of life-threatening incidents and the cost of operations without harming the environment. Consequently, biocompatible polymers have been introduced as nontoxic antifouling coating materials for surfaces, including poly(ethylene glycol) (PEG),[3] polyalkyloxazoline,[4] polyacrylate,[5] poly(2-hydroxyethyl methacrylate),[6] and polyacrylamide.[7] Among these, PEG has been widely used because of its high aqueous solubility, chain flexibility, and biocompatibility, resulting in antifouling and lubrication properties via steric repulsion and surface hydration.[8,9]

However, the immobilization of PEG onto target surfaces is a significant challenge due to the unique antifouling behavior of PEG itself. To date, these issues have primarily been addressed by surface-specific modifications, including the introduction of thiols for gold surfaces[10] and silanization.[11] Alternatively, a universal surface coating strategy based on catechol moieties adapted from mussel-adhesive proteins could provide versatile adhesion independent of the type of surface.[12] This versatility has been widely exploited in various applications, such as adhesives,[13] surface coatings,[14] hydrogels,[15] surface primers,[16,17] nanoparticle modification agents,[18] and sensors.[19] Similarly, the immobilization of PEG to the surface using the catechol moiety has been suggested in diverse formats, including terminal group modification,[20,21] grafting with catechol functional groups,[22,23] and the polymerization of catechol-functionalized monomers using PEG as a macroinitiator.[24,25] Among these strategies, the use of catechol-functionalized monomers offers a method to control the molecular weight, catechol content, and location of the catechol group in the polymer. However, most previous

Received: March 2, 2020
Revised: April 13, 2020

https://dx.doi.org/10.1021/acs.macromol.0c00481
Macromolecules XXXX, XXX, XXX−XXX

Scheme 1. Preparation of Catechol-Functionalized Polymer Films Presenting Antifouling Effects: (a) Mussel-Inspired Synthesis of Functional Monomer of Catechol Acetonide Glycidyl Ether (CAG), (b) Synthetic Scheme of Catechol-Functionalized Triblock Copolymers, and (c) Schematic of the Antifouling Surfaces Bearing Polymer Brushes and Polymer Loops against Model Protein Foulants

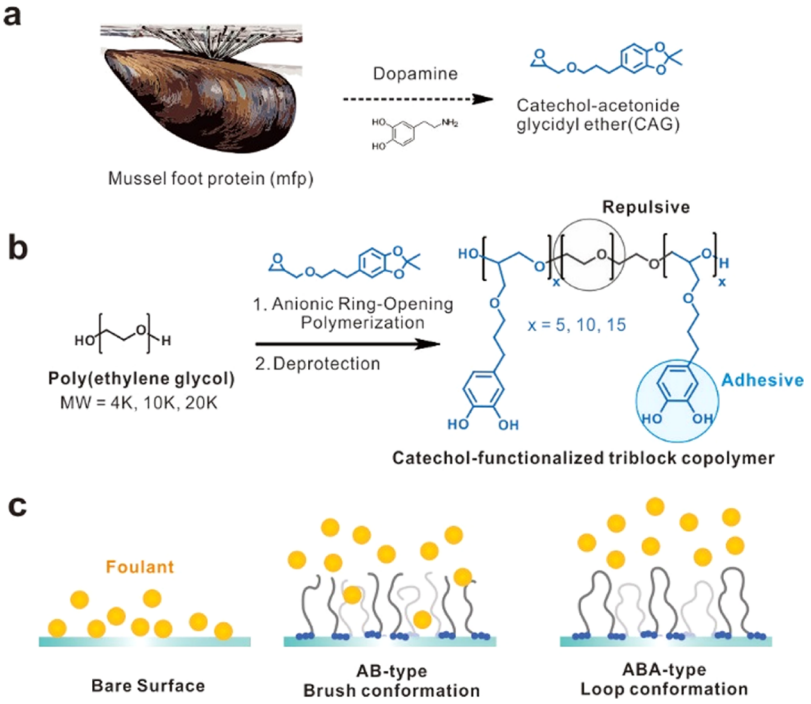

approaches have exploited rigid and hydrophobic catechol moieties incorporated into the flexible hydrophilic PEG backbone, which inevitably induces the segregation of the catechol functional groups from the main hydrophilic backbone, thus limiting the surface anchoring of the polymer chains.

Recently, ABA-type triblock copolymers forming a loop conformation have been actively explored as advanced antifouling coatings because of their large excluded volume and strong steric hindrance. Unlike traditional AB-type diblock copolymers, which form brushes, these triblock copolymers have displayed enhanced antifouling and lubrication properties.[22,26] Interestingly in nature, lubricin, which is an ABA-type triblock protein copolymer consisting of sticky end blocks and slippery midblock, is a major component of mammalian synovial fluids, and known to adopt a loop conformation on surfaces, displaying excellent lubrication and antifouling properties.[27,28] It is also of note that the cyclic polymers provide a superior steric stabilization of surfaces, antifouling, and lubricating behavior owing to the absence of the chain end.[29]

Despite successful early examples, the effects of the polymer composition and conformation have rarely been investigated, even though the length of the catechol units is known to affect their interactions with the surface and the surface-coating densities.[30] Thus, we herein study the antifouling properties of PEG-based block copolyethers functionalized with catechol moieties exclusively within the polyether framework (Scheme 1). For this purpose, we introduced a catechol-based epoxide monomer[31,32] into hydrophilic PEG as a versatile anchoring point with various composition and conformation to fully realize the antifouling properties. The anchoring of these polymers on surfaces was investigated by atomic force microscopy (AFM) and static contact angle measurements. The molecular-level interactions and antifouling properties of the polymer-coated surfaces were thoroughly evaluated using a surface force apparatus (SFA) and quartz crystal microbalance with dissipation (QCM-D). Furthermore, extensive atomistic molecular dynamics (MD) simulations were carried out to identify the fundamental molecular characteristics underlying the superior antifouling properties demonstrated by the triblock loop-like copolymer relative to those of the diblock brush-like copolymer. Finally, the antifouling properties of the polymer-coated surface were further studied via a cell attachment assay.

MATERIALS AND METHODS

Reagents. *p*-Toluene sulfonic acid monohydrate (*p*-TsOH), lithium aluminum hydride ($LiAlH_4$), epichlorohydrin (ECH), tetrabutylammonium bromide (TBAB), phosphazene base *t*-Bu-P_4 solution (0.8 M in hexane), bovine serum albumin (BSA), and toluene were obtained from Sigma-Aldrich. 3,4-Dihydroxyhydrocinnamic acid (C-COOH), 2,2-dimethoxypropane, anhydrous methanol, aluminum oxide, PEG, and poly(ethylene glycol) monomethyl ether (*m*PEG) were purchased from Alfa-Aesar. Diethyl ether and 50% sodium hydroxide aqueous solution were obtained from Daejung. Ethyl acetate, hexane, and methanol were purchased from SK Chemical. All deuterated NMR solvents, such as $CDCl_3$ and D_2O, were purchased from Cambridge Isotope Laboratories. All chemicals were of analytical reagent grade and were used without purification unless otherwise indicated.

Instruments. ^1H NMR spectra were recorded at 298 K with a VNMRS 400 spectrometer (Agilent Technologies, CA, USA) operating at 400 MHz using $CDCl_3$ and D_2O as the solvents. All spectra were measured using tetramethylsilane as an internal standard in the deuterated solvents. Size exclusion chromatography (SEC) measurements were performed using an Agilent 1200 series instrument with dimethylformamide (DMF) as an eluent at a flow

https://dx.doi.org/10.1021/acs.macromol.0c00481
Macromolecules XXXX, XXX, XXX−XXX

rate of 1.0 mL/min at 40 °C using a refractive index detector. Standard PEG samples (Agilent) were used for calibration to determine the number- and weight-average molecular weight (M_n and M_w). Matrix-assisted laser desorption and ionization time-of-flight (MALDI-TOF) mass spectrometry were performed using an Ultraflex III MALDI mass spectrometer (Bruker, Bremen, Germany). Thermogravimetric analysis (TGA) was performed on a TGA Q50 analyzer (TA Instruments, DE, USA). The surface morphologies of the polymer-coated surfaces were examined by AFM (NX-10, Park Systems, Suwon, Korea). The contact angle was determined using a Phoenix 300 goniometer (Surface Electro Optics Co. Ltd., Suwon, Korea). The surface interaction was studied using an SFA 2000 system (SurForce LLC, CA, USA). The real-time adsorptions of the polymer and protein were measured by a Q-sense E4 system (Biolin Scientific, Stockholm, Sweden). The mass and grafting density of each polymer adsorbed onto the surface were analyzed using QCM200 (Stanford Research System, CA, USA). Cell attachment was observed using an inverted microscope (IX73, OLYMPUS, Tokyo, Japan).

Synthesis of Acetonide-Protected Catechol Bearing an Epoxide Monomer. A mixture of 50% aqueous NaOH (80 mL, 1.00 mol, 16 equiv), ECH (23.3 g, 251.8 mmol, 4 equiv), and TBAB (1.01 g, 3.14 mmol, 0.05 equiv) was stirred vigorously at 0 °C. To this reaction mixture, 2,2-dimethyl-1,3-benzodioxole-5-propanol[18] (CA-OH, 13.11 g, 62.9 mmol, 1 equiv) was slowly added and stirred overnight. Excess water was added to dilute the reaction mixture and extracted with diethyl ether. The organic phase was dried with $MgSO_4$ and concentrated to obtain a pale-yellow, oily product. The crude product was purified using silica gel column chromatography with ethyl acetate/hexane (1:4 v/v) as the eluent to afford the catechol-functionalized monomer, CAG. CAG was distilled before polymerization to give the pure product. Yield: 81.6%. ^{1}H NMR (400 MHz, $CDCl_3$): δ [ppm] 6.59−6.47 (m, 3H), 3.63 (dd, J = 11.5, 3.1 Hz, 1H), 3.42 (qt, J = 9.3, 6.4 Hz, 2H), 3.31 (dd, J = 11.5, 5.8 Hz, 1H), 3.08 (td, J = 6.2, 3.3 Hz, 1H), 2.72 (t, J = 4.6 Hz, 1H), 2.57−2.48 (m, 3H), 1.85−1.63 (m, J = 13.3, 6.5 Hz, 2H), 1.58 (s, 6H). ^{13}C NMR (150 MHz, $CDCl_3$): 150.05, 148.15, 137.59, 128.38, 120.11, 111.28, 110.70, 74.20, 73.19, 53.55, 46.99, 34.73, 34.16, 28.37.

Synthesis of PCAG-*b*-PEG-*b*-PCAG Triblock Copolymers (ABA-Type Loop Polymers). A series of protected catechol-functionalized polymers were synthesized by anionic ring-opening polymerization (AROP) by varying the molar ratio of CAG and the molecular weight of PEG. Taking *L10K-10 as an example, PEG (1 g, MW 10,000, 0.1 mmol, 1 equiv) was added to a flask and dried at 100 °C for 3 h. After cooling the reaction flask to room temperature, it was purged with nitrogen, 3 mL of toluene was added, and heated to 60 °C. Phosphazene base, *t*-Bu-P_4 (0.25 mL, 0.2 mmol, 2 equiv), was added, and the mixture was stirred for 30 min. Then, CAG monomer (0.528 g, 2 mmol) was slowly added, and the mixture was stirred overnight. The polymerization was quenched by the addition of benzoic acid, and the resulting polymer was passed through a pad of alumina with THF. The solution was precipitated by pouring into hexane and diethyl ether to give PCAG-*b*-PEG-*b*-PCAG. The degree of polymerization was calculated from the NMR data using the following equation: number of repeating units (CAG) = [226.96 (number of repeating units in the PEG macroinitiator) × 4 (number of protons on PEG)]/[29.9 (integration value) × 2 − 7 (number of protons on CAG)]. M_n = 264.32 (molecular weight of CAG) × 17.19 (number of CAG repeating units) + 10,000 (molecular weight of PEG) = 14,543.66 g/mol.

Removal of the Acetonide Group. The protected block copolymer (100 mg) was stirred in 0.8 mL of hydrogen chloride solution (32%) and 9.2 mL of methanol at 40 °C. The mixture was stirred while open to the atmosphere to allow acetone to escape from the reaction. After 3 h, the excess solvent was removed using a rotary evaporator, and the product was dried using a vacuum oven. The concentrated product was precipitated into cold diethyl ether. Yield: quantitative.

Thermogravimetric Analysis. The thermal stability of the polymer was characterized by TGA. The measurements were conducted on a TG50 instrument under a nitrogen atmosphere within the temperature range of 25−500 °C at a heating rate of 10 °C/min.

Differential Scanning Calorimetry. Differential scanning calorimetry (DSC) was carried out under a nitrogen atmosphere in the temperature range of −80 to 65 °C and at a heating rate of 10 K/min (Q200 model, TA Instruments, USA).

Static Contact Angle Measurements. The static contact angles of water on the coated substrates were measured to analyze surface modification. A variety of substrates, including SiO_2, polystyrene, poly(ether ether ketone), acrylate, poly(ethylene terephthalate), TiO_2, Au, and glass, were cleaned prior to use and then incubated for 1 h in 10 mg/mL polymer solution in methanol at room temperature. After incubation, each substrate was washed three times with methanol and dried with nitrogen. All samples were analyzed at least five times, and the average value with the standard deviation as the error range is reported.

Interaction Force Measurements between the Polymer-Coated Surfaces Using SFA. A SFA 2000 (SurForce LLC, Santa Barbara, CA, USA) was used to measure the interaction forces between the polymer-coated surfaces. The interaction forces were measured with two sets of symmetric polymers (i.e. loops, and brushes). To prepare the polymer-coated surfaces, freshly cleaved back-silvered mica (Grade #1, S&J Trading, Floral Park, NY, USA) was glued onto a cylindrical glass disk using an optical adhesive (NOA 81, Norland Products, Inc. Cranbury, NJ, USA). Then, each polymer solution (10 mg/mL in methanol) was added dropwise onto the mica surface and allowed to stand for 10 min. After standing, the surface was thoroughly washed with methanol to remove unbound molecules. The polymer-coated surfaces were transferred into the SFA chamber with a crossed-cylinder geometry, and 50 μL of the corresponding buffer was injected between the opposing surfaces. The system was equilibrated for 1 h prior to the measurements. The two surfaces were brought into contact by a motor connected to the lower surface and then separated. The absolute distance (D) and interaction force (F) between the mica surfaces were measured by using multiple beam interferometry.[47] To investigate the antifouling properties of the polymer-coated surfaces, interaction force measurements in the presence of the following intervening fluids were performed in series: (i) 10 mM phosphate-buffered saline (PBS), (ii) BSA solution (1 mg/mL in 10 mM PBS), (iii) BSA solution (after 1 h of incubation), and (iv) 10 mM PBS. Before the last force measurement with 10 mM PBS, the surfaces were thoroughly rinsed with deionized (DI) water to remove loosely bound BSA. All force measurements were repeated at least three times, and different contact points for each buffer to confirm the reproducibility of the measurements. The friction force measurements between the polymer-coated surfaces were performed using a bimorph slider attachment[48] with a sliding speed of ∼10 μm/s at various applied loads.

Polymer and Protein Adsorption Tests Using QCM-D. The real-time surface adsorption was measured using a gold-coated sensor (QSX 301). The sensor was transferred to a standard Q-sense flow module and equilibrated using 1× PBS before polymer injection. The flow rate was 600 μL/min, and the temperature was controlled at 25 °C for all experiments. The Voigt model was adopted to calculate the mass of adsorbed proteins with Qtools software (Q-Sense, Sweden). The density of the adsorbed BSA layer was assumed to be 1200 kg/m^3, the fluid density was assumed to be 1000 kg/m^3, and the fluid viscosity was assumed to be 0.001 kg/ms.

Polymer Grafting Density Measurement Using QCM. The mass of the polymer layer in the dry state was measured by a QCM (Stanford Research System, QCM200). For each polymer solution (10 mg/mL in methanol), the solution was added dropwise onto the chip, and the chip was incubated for 10 min and then rinsed with methanol to remove any unbound polymer. The frequency shift after surface coating was measured, and the dry mass was calculated using the Sauerbrey equation, $\Delta F = -C_f \times \Delta m$, where ΔF is the time-resolved changes in resonance frequency (Hz), C_f is the sensitivity factor of the crystal, and Δm is the mass difference per unit area (μg/cm^2).[49] The grafting density, σ, was calculated using $\sigma = mN_A/M_n$,

https://dx.doi.org/10.1021/acs.macromol.0c00481
Macromolecules XXXX, XXX, XXX−XXX

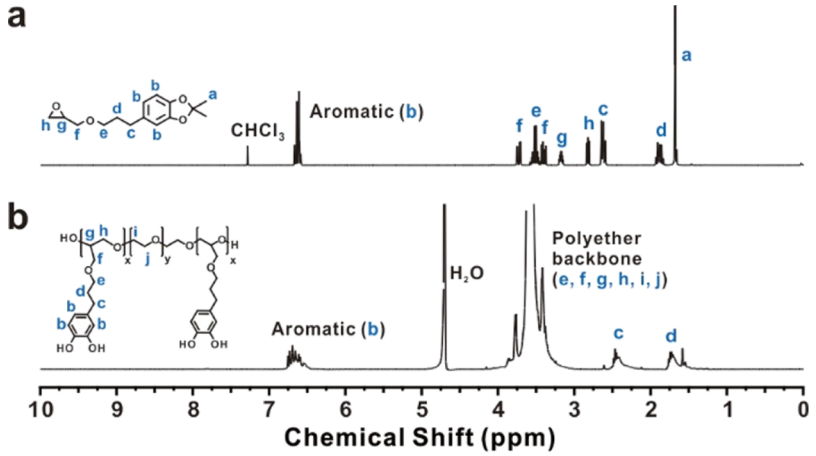

Figure 1. ^{1}H NMR spectra of (a) CAG monomer and (b) catechol-functionalized triblock copolymer (L10K-10 in Table 1).

where N_A is Avogadro's number and M_n is the number-average molecular weight of the polymer.

Raman Spectroscopy. Raman spectroscopy (XploRA PLUS, HORIBA, Japan) was employed to evaluate the intensity of hydrogen bonding between bulk water and the polymer surface. Before the Raman spectroscopy measurement, the samples were fully immersed in DI water for 6 h to induce the full hydration over the surface. The samples were exposed to the laser with a wavelength of 532 nm under the optimized measurement condition. After that, the collected Raman spectrum was fitted with the Gaussian model using OriginPro software (OriginLab Co., Northampton, MA, USA). The corresponding vibrational stretching modes of water molecules were deconvoluted into five distinct vibrational modes of DAA, DDAA, DA, DDA, and free OH.[50]

MD Simulations. The MD simulations were performed with the 2.12 version of the NAMD MD package with the CHARMM force fields.[51,52] The initial structures of the CAG homopolymer, PCAG-*b*-PEG, PCAG-*b*-PEG-*b*-PCAG, and mica surface were constructed using the Materials Studio software package.[53] The polymers were then solvated with water (based on the TIP3P water model)[54] and with NaCl to reach an ionic concentration of 0.15 M for the bulk phase and were then combined with the mica surface to build the target confined systems with the help of the VMD package.[55] The confined systems were periodic only in the *x*- and *y*-directions (i.e., on the solid surface). The electrostatic interactions between atoms were calculated with the particle mesh Ewald[56] for bulk systems and with the multilevel summation method[57] for the confined systems. All systems were initially equilibrated in the isothermal−isobaric (*NPT*) ensemble at T = 300 K and P = 1 atm using the Langevin thermostat and barostat. The configurations of the fully equilibrated system were subsequently subjected to canonical (*NVT*) MD simulations corresponding to T = 300 K and P = 1 atm for the production run. To extract the essential structural characteristics of the protective polymers covering the solid surface, the brush and loop polymers were simulated with one chain end and with both chain ends (i.e., the anchoring catechol units), respectively, being fixed on the surface. To obtain statistically meaningful structural properties for the loop polymers, four representative fixed distances between the two chain ends were adopted in the simulation, namely, 1.28 (0.170), 3.60 (0.344), 5.44 (0.321), and 8.15 (0.165) nm, where the values in parentheses indicate the relative probabilities, according to the two-dimensional Gaussian distribution $P(r) \approx r\, e^{-r^2/\langle r^2\rangle}$ for the chain end-to-end distance r in conjunction with the mean-square chain end-to-end distance $\langle r^2\rangle \approx 34.5$ nm^2 obtained from the PEG-10K bulk simulation. All the properties of the loop polymer (L10K-10) reported here are based on the statistical average accounting for the respective probabilities of the four representative loop systems.

In Vitro Cell Adhesion and Cytotoxicity Test. The model cell, human dermal fibroblasts (CC-2511, Lonza, Switzerland), were maintained at 37 °C in a humidified incubator under 5% CO_2 in Dulbecco's modified Eagle medium supplemented with 10% fetal bovine serum (Gibco Life Technologies, USA) and 1% penicillin/streptomycin antibiotics (Gibco Life Technologies, USA). Before cell culture, the samples were washed with PBS three times. The samples were placed on the 12-well culture plate, and cells were seeded over the samples with a density of 1 × 10^4 cells/mL. Also, two control experiments were followed; positive control without the sample and negative control with 20% dimethyl sulfoxide to induce cell death. The cells were incubated with the samples for 24 h. To evaluate the cell repelling property, the cell-cultured samples were carefully moved to the new cultures. Loosely attached cells were washed with PBS, and the number of cells attached to each sample was calculated using the conventional hemocytometer. For evaluation of the cytotoxicity, each well was treated with a Cell Counting Kit (CCK, Donginbiotech, Korea) and incubated about 1 h. Then, the change of viability due to each sample was tracked by measuring the optical density at a wavelength of 450 nm. The optical density was normalized to the positive control to determine the cytotoxicity of each sample.

Cell Attachment Test. The L929 mammalian fibroblast cell line was used in the cell attachment test. Each glass substrate (1 × 1 cm^2) was placed in a 24-well cell culture plate and sterilized by exposure to UV irradiation for 30 min and washed three times using 70% ethanol. After equilibration with 1× PBS and RPMI media for 30 min, L929 cells were seeded in the cell culture plate containing the polymer-coated substrates at a density of 1 × 10^5 cells per substrate. The cell culture plate was incubated for 24 h in 5% CO_2 at 37 °C. After 24 h, the glass substrates were washed three times with 1× PBS to remove any nonadherent cells, transferred to new cell culture plates, and examined by optical microscopy. A bare glass substrate was used as a control.

RESULTS AND DISCUSSION

Polymerization. The synthesis of the CAG and PEG-initiated block copolymer was carried out according to the method described in the Materials and Methods section and the Supporting Information. The successful synthesis of CAG was confirmed via NMR spectroscopy and electrospray ionization mass spectrometry (ESI-MS) (Figures 1 and S1−S4). After the synthesis of CAG, catechol-functionalized triblock copolymers were synthesized by AROP using PEG as a macroinitiator. The use of a conventional base (i.e. CsOH) resulted in a low conversion due to the steric hindrance of the bulky side groups of the CAG monomer. Moreover, the increased reaction temperature resulted in the degradation of the acetonide protecting groups during polymerization (Figure S5 and Table S1). Thus, we employed a metal-free phosphazene base, which exhibits a high basicity

https://dx.doi.org/10.1021/acs.macromol.0c00481
Macromolecules XXXX, XXX, XXX−XXX

and low nucleophilicity, allowing the polymerization of the CAG monomer to be achieved at a mild temperature.[33] As shown in Figure S6, the representative ^{1}H NMR spectra of the triblock copolymer showed peaks corresponding to the aromatic ring (6.51−6.91 ppm) and carbon chain (1.82 and 2.55 ppm) of the catechol moieties and polyether backbone and PEG segments (3.24−4.04 ppm). Moreover, the acetonide groups were stable under the polymerization conditions (1.66 ppm). As a control, brush-like diblock copolymers were also synthesized by AROP using methoxy-PEG (*m*PEG) as an initiator under identical reaction conditions.

The characterizations of the synthesized polymers are listed in Table 1. Because of the hydrophobicity of the catechol block, the molecular weight measured by SEC was relatively smaller than that measured by ^{1}H NMR spectroscopy. However, the increased molecular weight upon polymerization with a narrow distribution confirmed the successful synthesis of the catechol-functionalized block copolymers (Figures S7 and S8). Because the molecular weight of CAG is six times higher than that of ethylene oxide, which is the monomer of PEG, it is difficult to identify the presence of CAG in the triblock copolymers directly from the MALDI-MS spectra (Figure S9). Alternatively, the CAG homopolymer was synthesized under identical reaction conditions, and the spacing of the signals corresponded to the mass of the respective monomers as expected.

Table 1. Characterizations of the Catechol-Functionalized Polymers Prepared in This Study

polymer	composition[a]	$M_{n,NMR}$[a] (g/mol)	$M_{n,SEC}$[b] (g/mol)	$Đ$[b]
*L4K-10	$PCAG_7$-*b*-PEG_{91}-*b*-$PCAG_7$	7400	4850	1.03
*L10K-5	$PCAG_4$-*b*-PEG_{227}-*b*-$PCAG_4$	11,850	10,900	1.10
*L10K-10	$PCAG_9$-*b*-PEG_{227}-*b*-$PCAG_9$	14,550	13,640	1.08
*L10K-15	$PCAG_{12}$-*b*-PEG_{227}-*b*-$PCAG_{12}$	17,290	14,940	1.32
*L20K-10	$PCAG_9$-*b*-PEG_{453}-*b*-$PCAG_9$	24,500	22,700	1.04
*B5K-5	PEG_{114}-*b*-$PCAG_4$	5930	5390	1.09
*B5K-10	PEG_{114}-*b*-$PCAG_9$	7370	6890	1.12
*B5K-15	PEG_{114}-*b*-$PCAG_{12}$	8960	6980	1.14

[a]The M_n and the composition of the block copolymer were determined via ^{1}H NMR spectroscopy in $CDCl_3$. [b]$Đ(M_w/M_n)$ was measured by SEC analysis with PEG standards in DMF. [*L(*X*)-(*Y*) (protected loop polymer) or *B(*X*)-(*Y*) (protected brush polymer) in accordance with the molecular weight.].

The incorporation of catechol moieties into the block copolymer was also confirmed by TGA and DSC (Figure S10). Bare PEG, *L10K-5, *L10K-10, and CAG homopolymer ($PCAG_{20}$) were thermally stable up to 300 °C. The weight percentages of the residues after thermal decomposition of these polymers at 500 °C were 2.0, 4.3, 6.9, and 15.2%, respectively. The residue weights increased according to the content of CAG due to the higher thermal stability of the catechol moieties. In the DSC curve, the catechol-functionalized block copolymers showed a single glass-transition temperature (T_g) due to the high miscibility of the comparatively small catechol blocks. The T_g increased with increasing content of the catechol moiety due to the high rigidity of the side chains. These results demonstrate that catechol groups were successfully incorporated into the block copolymer.

After polymerization, the acetonide-protecting groups were removed by treatment with hydrochloric acid, revealing free catechol groups. The successful deprotection was confirmed by

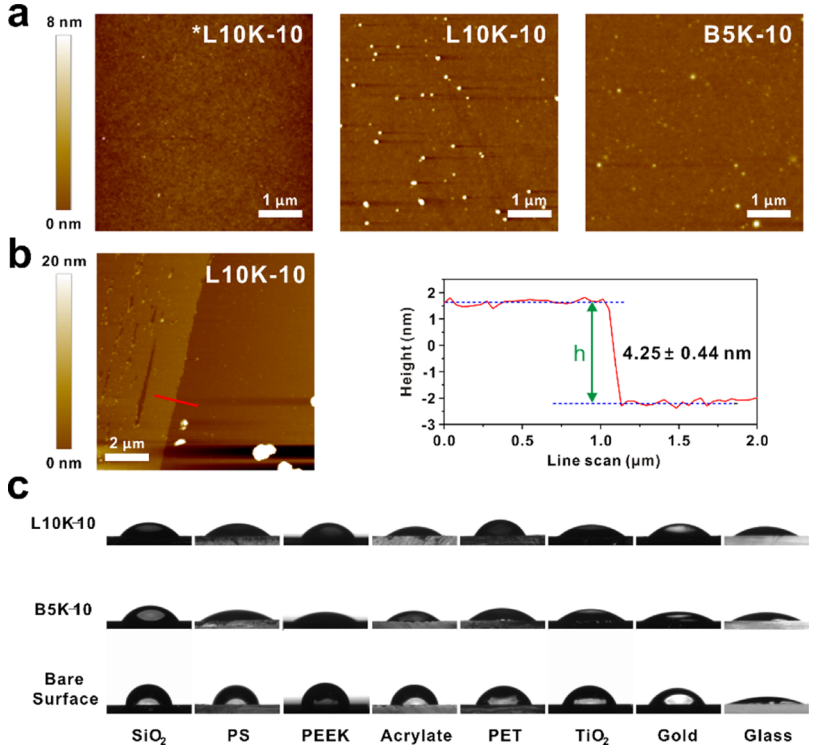

Figure 2. (a) Topographic AFM images of *L10K-10, L10K-10, and B5K-10 coatings on silicon wafers (polymer concentration: 10 mg/mL in MeOH). (b) Scratch test of L10K-10 coating with the corresponding AFM image and scan profile. (c) Static contact angles of water droplets on various surfaces: loop polymer (L10K-10)-treated surfaces, brush polymer (B5K-10)-treated surfaces, and bare surfaces.

https://dx.doi.org/10.1021/acs.macromol.0c00481
Macromolecules XXXX, XXX, XXX−XXX

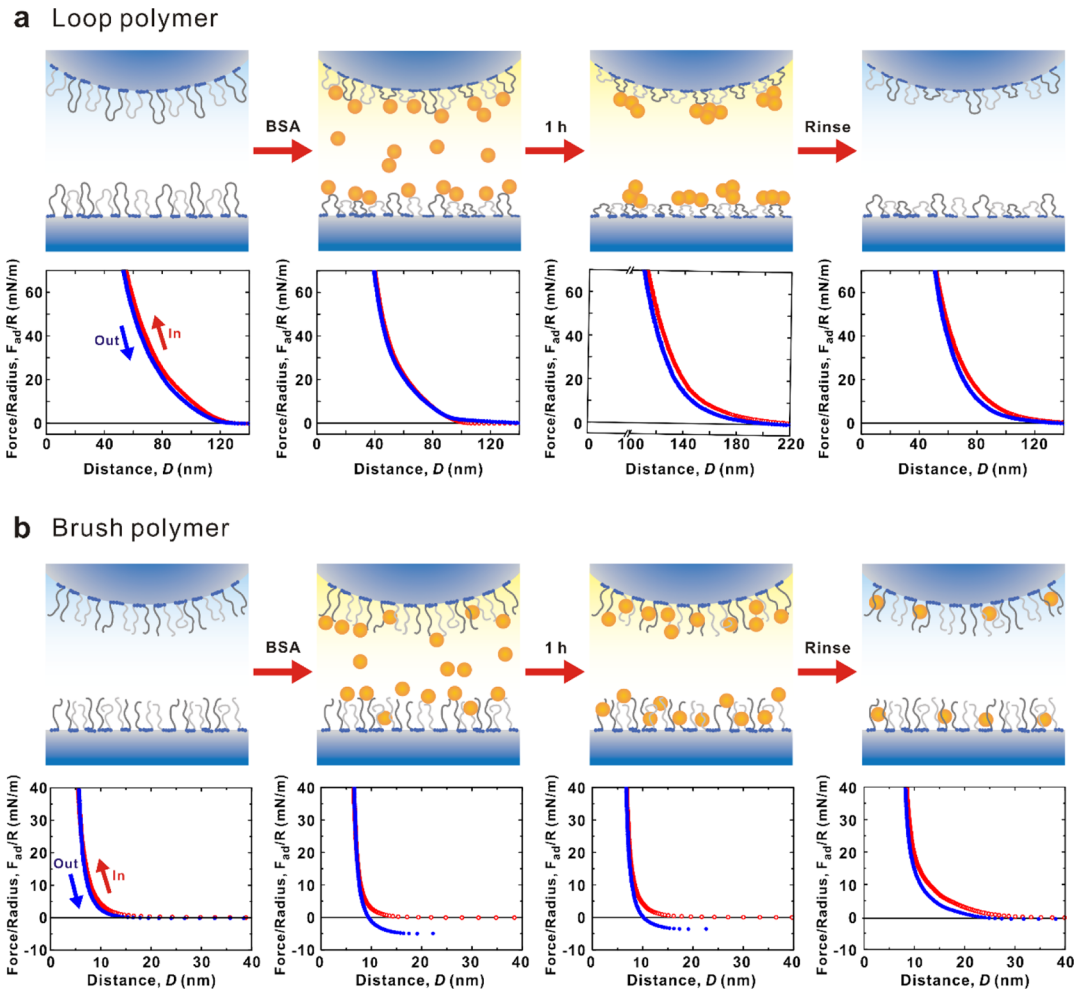

Figure 3. Schematics depicting the antifouling assessment of the polymer films using a SFA and force−distance profiles between the two polymer films. Force−distance profiles between the (a) L10K-10 and (b) B5K-10 polymer films with the following treatment sequences: 10 mM PBS, BSA solution with 1 h incubation, and rinsing with 10 mM PBS.

the disappearance of the signal of the methyl protons at 1.58 ppm in the ^{1}H NMR spectrum, while PEG midblock did not show any sign of degradation (Figures 1 and S11). Moreover, the catechol moieties in the deprotected polymer, for example, L10K-10, were rapidly oxidized in pH 8.5 buffer within 12 h, further indicating the presence of free catechol groups (Figure S12).

Surface Characterization. Using a simple solution dipping method, the catechol block of each copolymer induced the adsorption of polymers on the substrate. The morphology and the nanostructure of the polymer-coated surfaces were studied by AFM. Both loop and brush copolymers were uniformly distributed on the surface of the silicon wafers, while the protected polymer (i.e., *L10K-10) was rinsed away, revealing the critical role of the free catechol moieties in the anchoring of the polymers on the substrate (Figure 2a). When the scratch test of L10K-10- and B5K-10-coated surface was conducted, the thickness of the loop and brush layer underneath was determined to be 4.25 ± 0.44 and 2.32 ± 0.33 nm, respectively (Figure 2b). In addition, the ellipsometry measurement supported the formation of the polymer layer of loop and brush coatings in 4.22 ± 0.07 and 5.33 ± 0.48 nm, respectively. Meanwhile, it should be noted that the surface morphology of the polymers was affected by the drying condition and rinsing solvent (Figure S13).

The versatile surface binding ability was also confirmed by measuring the static contact angle of water droplets after coating various substrates with the prepared polymers. Regardless of substrate hydrophilicity and hydrophobicity, the contact angle of the droplet on each coated surface was within a similar range of values, which demonstrated the potential of the catechol-functionalized polymer as a substrate-independent universal coating material (Figures 2c and S14).

Interaction Force Measurements. The interaction forces of the loop and brush polymer-coated surfaces were measured using an SFA (Figure 3). SFA has been widely used for measuring the absolute distances and interaction forces between two macroscopic surfaces with an ultimate resolution of 0.1 nm and 10 nN, respectively.[34] In this study, to investigate the antifouling effect of two polymers in terms of the protein adsorption, BSA was used. BSA is a well-known foulant that is commonly used as a model protein because it can easily adsorb onto many different surfaces through nonspecific interactions.[35] We prepared each polymer-coated surface symmetrically (loop vs loop and brush vs brush), and the force measurements were conducted by changing the intervening buffers in the following order: 10 mM PBS, BSA solution, and 10 mM PBS after cleaning the surfaces.

In the PBS solution, both the loop and brush polymer-coated surfaces exhibited purely repulsive force profiles,

https://dx.doi.org/10.1021/acs.macromol.0c00481
Macromolecules XXXX, XXX, XXX−XXX

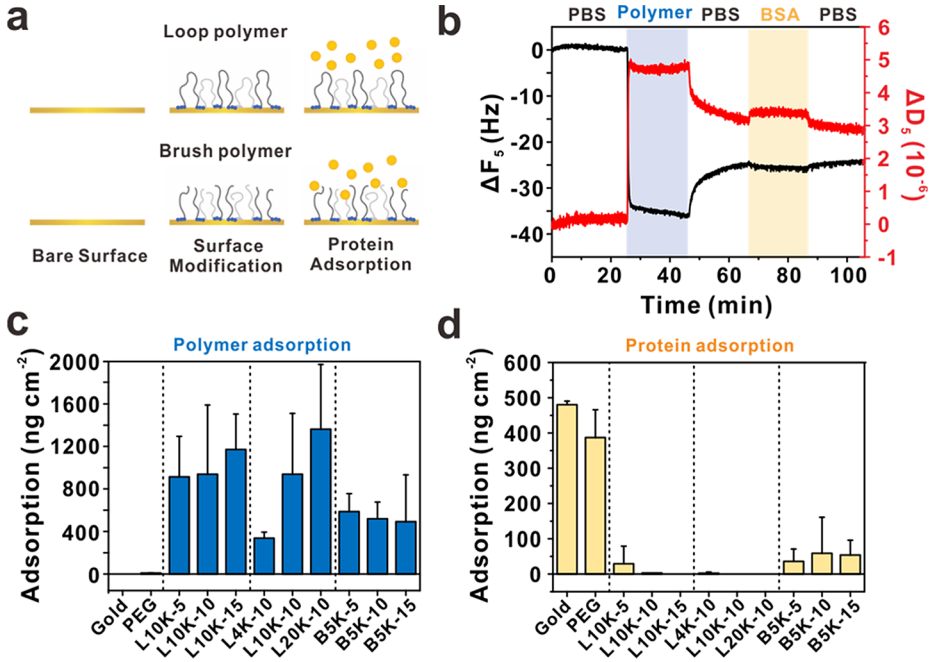

Figure 4. (a) Schematic of the antifouling test by QCM-D. (b) Changes in frequency and dissipation associated with the adsorption of the polymer (L10K-10) and protein on a gold sensor. (c) Adsorption of various polymers on bare gold surfaces. (d) Adsorption of BSA on bare gold surfaces and those coated with various polymers.

attributable to the "steric repulsion" of the polymers. The loop polymer showed a thicker steric wall distance (defined as D at $F/R \approx 70$ mN/m); the average D_{sw} was 48.6 ± 6.5 nm and that of the brush polymer was 6.9 ± 1.8 nm. This result indicated that the loop polymer showed greater resistance than the brush polymer to compression. Because both ends of the polymer loop are immobilized onto the surface, forming a closed structure, there are fewer opportunities for interpenetration, and it is less able to tilt or lie flat upon compression, which can result in a thicker D_{sw} compared to that of the brush polymer. Considering that the Debye length of 10 mM PBS is 0.76 nm, the significantly larger decay length (~22.9 for the loop and ~6.3 for the brush) of the force−distance curve also supports that steric contributions are critical during the approach (Figure S15).

Immediately after the injection of the BSA solution, the interaction force between the loop polymer-coated surfaces increased in repulsion, and D_{sw} decreased from 55 to 40 nm. The decreased D_{sw} can be attributed to the collapse of the loop polymers by instant adsorption of the BSA onto both surfaces. However, the D_{sw} significantly increased to 112 nm after 1 h of resting. Repulsion was observed at a separation distance of 190 nm, which was considerably farther than the case without the BSA due to the flocculation of the BSA by strong hydrophobic interactions.[36,37] After rinsing the surfaces with DI water, the force measurements in PBS showed a marked decrease in repulsion and D_{sw} returned to 55 nm, indicating high reversibility.

Unlike the loop polymer-coated surfaces, the following force profiles were measured between brush polymer-coated surfaces upon injection of BSA: (i) during the approach, in which the BSA did not affect the repulsive force between the surfaces and (ii) during the separation, in which an adhesion force, F_{ad}, of −5.0 mN/m was measured. The measured adhesion force appears to be mediated by the bridging of the BSA molecules, which penetrated between the gaps in the brush polymer on the opposing surfaces.[38,39] Because of the fast dynamics, including the high mobility and flexibility of the brush chain ends, the BSA has fewer chances to interact with the protein and aggregate. Thus, the BSA tended to be adsorbed between the brush polymer chains rather than stacked on the surfaces, while the BSA could be easily adsorbed and aggregated on the loop-coated surfaces because there were insufficient spaces to penetrate.[37,40] The adhesion force (F_{ad} = −3.6 mN/m) and force−distance profile after 1 h of resting nearly corresponded to the force measurements made immediately after BSA injection. Hence, the brush polymer-coated surfaces were structurally stable and did not show aggregation of the BSA. After thoroughly rinsing the surfaces with DI water, the adhesion force disappeared and D_{sw} increased to ~8.7 nm in PBS, indicating much more repulsion than was initially measured in PBS during the approach. It has been previously shown that the BSA can penetrate into the polymer brush layer, resulting in a slight increase in the height of brush polymer,[41,42] which exactly matches to our results. Thus, considering the fact that (i) the size of BSA is sufficiently small (Figure S16) and (ii) the PEG brush is highly fluctuating because of its end mobility (see additional movies in the Supporting Information), we believe that the BSA remaining in the gaps in the brush polymer led to a decrease in the chain mobility (which may prevent the polymers from tilting) even after thorough rinsing of the BSA on the surfaces.

Adsorption of the Polymer and Protein. The QCM-D technique was employed to monitor the real-time adsorption of the polymers and proteins on the surfaces (Figure 4). First, the gold sensor was equilibrated using 10 mM PBS, and polymer solution (1 mg/mL) was applied for 30 min. The introduction of the polymer generated a negative frequency shift, indicating an increase in mass at the surface. During this phase, the steep slope of the ΔD versus $\Delta F/n$ plot (7.7×10^{-7}/Hz) suggested that the adsorbates form a viscoelastic layer with a considerable amount of energy dissipation (Figure

https://dx.doi.org/10.1021/acs.macromol.0c00481
Macromolecules XXXX, XXX, XXX−XXX

S17).[24] The loosely bound polymers were removed by rinsing, and the BSA solution was introduced. As shown in Figure 4b, the frequency decreased and recovered fully or partially after the rinsing step. Considering the viscoelastic nature of the polymer-coated on the surface, the Voigt model was used to calculate the mass of both the polymer and protein (Figure 4c,d).

As expected, the catechol-functionalized block copolymers were successfully coated onto the gold surface, while it is difficult to immobilize pristine PEG on the surface (9.5 ng/cm^2). Therefore, pristine PEG alone was not effective at inhibiting the binding of protein because of its limited surface adsorption. The brush polymer effectively inhibited protein adsorption and exhibited an 8-fold lower protein uptake (59 ng/cm^2 for B5K-10) than that of non-functionalized PEG. Despite the lower grafting density of L10K-10 compared to that of B5K-10, the molecular weight and the number of anchoring blocks of the loop polymer are twice those of the brush polymer (Table S2); thus, the loop polymer forms a denser layer than the brush polymer. A markedly higher suppression of protein adsorption was observed with the loop polymer compared with the brush polymer (approximately 0 ng/cm^2 except for L10K-5), revealing the critical role of the topology in enhancing the antifouling properties. Similarly, Hawker and co-workers reported that the frictional force of loop polymers was reduced compared to that of brush polymers due to the lower interpenetration between the polymer chains.[22] However, both the loop and brush polymer-coated surfaces showed almost equal coefficients of friction in this study (μ = 0.27, Figure S18), which is not surprising because the degrees of hydration (which determines the coefficient of friction) of the loop and brush polymer should be similar. More importantly, the applied pressure (P) at which the mica surface is severely damaged was approximately 8 times higher for loop polymer-coated surfaces (37.8 MPa) than that with the brush polymer (4.4 MPa). This result indicates that the loop polymer has greater stability and resistance to certain types of mechanical stresses (e.g., compressive, shear, and bearing stress) compared to the brush polymer, which was described in the SFA measurement section. The benefit of loop conformaiton can be explained with the absence of chain ends, significantly affecting the properties of surface-grafted polymers,[43] which in turn supports the superior antifouling effects and the enhanced shear stability of loop polymers presented in this study.

Independently, we used Raman spectroscopy to investigate the differences in the hydration dynamics of water molecules at the surface of polymer coating.[44] In particular, the orientation and the number of the hydrogen bonds formed between water molecules and neighboring molecules could influence the vibrational stretching modes of water molecules; for example, four types of hydrogen bonding exist, including a conventional strong DDAA (double donor−double acceptor) mode and non-conventional weak modes of DA (single donor−single acceptor), DAA (single donor−double acceptor), and DDA (double donor−single acceptor), where D denotes a hydrogen bonding donor, and A denotes a hydrogen bonding acceptor (see detailed conformations in Figure S19). Deconvolutions of these different vibrational modes of water molecules with L10K-10 or B5K-10-coated surfaces were evaluated. Interestingly, the portion of DA was the most significant in both surfaces because the number of bound water molecules per repeating unit of PEG was estimated to be one according to NMR relaxation study.[45] In accord with this observation, the ratio of the hydrogen bond and water on the polymer-coated surface was similar regardless of the conformation of the polymer in MD simulation (Figure S20). In general, both L10K-10 and B5K-10 showed similar conformational distributions of hydrogen bonding, which indicates that the polyether-coated surface shows a similar level of surface hydration regardless of the conformation of polymers.

Furthermore, the effect of the composition on the antifouling properties was studied using different lengths of PEG midblock. Although the mass of the adsorbed polymer increased as the molecular weight of PEG increased, for example, from 337 ng/cm^2 for L4K-10 to 1362 ng/cm^2 for L20K-10, the change was not entirely proportional to the molecular weight. For comparison, the dry mass and surface grafting density (σ) of polymers with different molecular weights of PEG (L4K-10, L10K-10, and L20K-10) were measured using a QCM-D (Table S2). The polymer with the longer PEG macroinitiator shows a lower surface grafting density (0.82−0.15 chains/nm^2) due to higher steric hindrance; thus, the magnitude of the increase in mass with increasing molecular weight was decreased.[29] However, the effect of the molecular weight of PEG was quite small due to the excellent intrinsic antifouling properties of PEG.

In addition, a quantitative assessment of the changes in the protein adsorption and antifouling properties as a function of the number of catechol units was conducted. Previously, it was found that increasing the number of catechol units increased the binding affinity to the surface, while in some cases, a large number of free catechol units unbound to the surface facilitates protein adsorption, hence diminishing the antifouling efficiency.[24,30] In this study, however, the polymer and protein adsorption with various anchoring block lengths did not significantly vary, implying that the length of the catechol block is sufficient to immobilize the polymers onto the surface while maintaining the antifouling effect of PEG without any disturbances from the catechol block.

MD Simulation. A comprehensive understanding of the superb antifouling features of the loop-like triblock copolymer in comparison to the brush-like diblock copolymer requires in-depth elucidation of the basic molecular characteristics behind the macroscopic observations, which will provide a further basis for the systematic characterization and development of advanced antifouling polymers in the future. In this respect, we first specify the representative structural and dynamic factors that are primarily responsible for determining the antifouling efficiency of the polymer and protecting the solid surface from the foulants, that is, (i) the average molecular surface area effectively covering the solid surface, (ii) the areal fluctuation, and (iii) the two-dimensional chain mobility on the solid surface. The first factor characterizes the average surface coverage by the protective polymer against unfavorable adsorption of the foulants from the bulk phase. Moreover, the degree of areal fluctuation (i.e., the second factor) is critical in determining the protective efficiency of the polymer. Generally, a larger fluctuation in the effective molecular area would lower the efficiency because it increases the chance for contaminant adsorption onto temporally exposed uncovered areas during areal fluctuations (this feature can be readily understood by considering the increased chance of getting wet when repeatedly folding and unfolding an umbrella in the rain). The third factor also influences the protective efficiency because the movement of antifouling agents from one place to

https://dx.doi.org/10.1021/acs.macromol.0c00481
Macromolecules XXXX, XXX, XXX−XXX

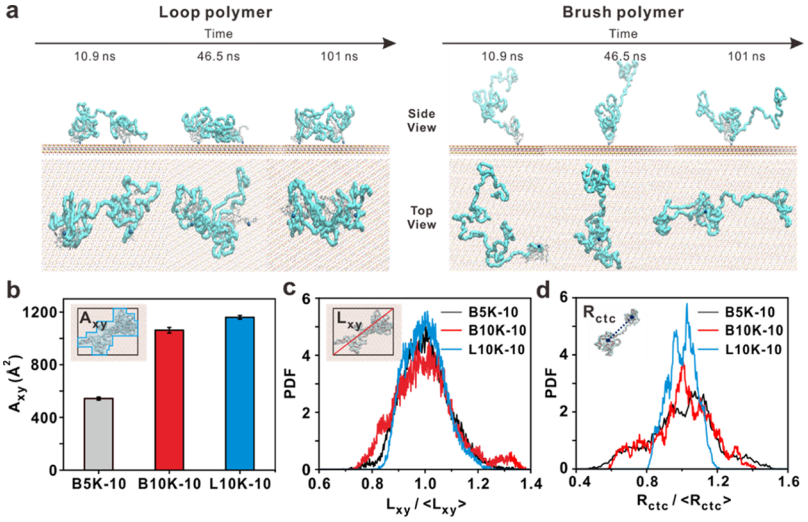

Figure 5. (a) Atomistic snapshots taken at different times from the 200 ns MD simulations of B10K-10 and L10K-10 on the mica surface as represented in side-on and top views. The anchoring atoms are highlighted as blue spheres, and water molecules and ions are omitted for clarity. (b) Comparison of the effective molecular surface area, A_{xy}, projected onto the solid surface in the *xy*-plane by the brush (B5K-10 and B10K-10) and loop (L10K-10) copolymers. Probability distribution function of (c) the representative diagonal chain dimension, L_{xy}, and (d) the chain center-to-center distance, R_{ctc}, connecting the two centers of mass of bisected chains for each system.

another on the solid surface would provide an opportunity for the bulk contaminants to adsorb onto a region that was protected but has been exposed (this can be understood by considering the increased tendency of getting wet if we move the umbrella around our body).

Based on these basic molecular aspects, we can consider the result of the simulation. Figure 5a displays atomistic snapshots obtained from the MD simulations for the brush (B10K-10) and loop (L10K-10) polymers on the mica surface, illustrating the distinctive structural features of these two types of polymers. Overall, the loop polymer exhibits a relatively larger projection area onto the solid surface (*xy*-plane) and a lesser degree of conformational (chain size and orientation) changes with time than the brush polymer, stemming from the geometrical constraint of having two fixed chain ends, which effectively forces the main PEG block of the loop to stay closer to the surface. As noted above, these structural characteristics are important factors in determining the protective efficiency of the polymer against foulant adsorption from the bulk material onto the solid surface. Specifically, the larger average molecular surface area of the loop polymer is essentially responsible for its protective efficiency being higher than that of the analogous brush polymer; a quantitative comparison between these polymers is presented in Figure 5b.

Furthermore, in contrast to the brush polymer, which exhibits larger and faster conformational variations with time because of its free chain end, the loop polymer maintains a rather stable overall structure without significant changes in size or orientation (see additional movies in the Supporting Information). This feature can be directly seen from the relatively narrower distributions for the loop polymer compared to those of the brush polymer with respect to certain representative chain dimensions (i.e., the diagonal chain dimension (L_{xy}) in the *xy*-plane and the chain center-to-center distance (R_{ctc}) connecting the two centers of mass formed by dividing chains into two equal fragments) (Figure 5c,d).[46] In addition, the presence of the anchoring CAG units at each of the two chain ends in the case of the loop polymer not only provides robust structural stability but also diminishes the diffusive chain mobility on the solid surface, thus improving the protective efficiency. Taken together, these features are the basic molecular characteristics behind the enhanced antifouling efficiency of the loop polymer compared to the corresponding brush polymer, as observed experimentally in this study.

Additionally, the magnitudes of the attractive (negative) interaction energies between the CAG homopolymer and the solid surface were determined with respect to the number of CAG units (Figure S21). As expected, with increasing CAG units, the magnitude of the interaction increases (although not strictly proportionally due to the structural constriction between neighboring CAG units), thus enhancing the binding affinity between the protective polymer and the solid surface (see Figure S22 for the interaction energy of a single catechol unit with the mica surface in comparison to that of phenol).

In Vitro Cell Adhesion and Cytotoxicity Test. The antifouling properties of the catechol-functionalized polymers were demonstrated by using human dermal fibroblasts cell, CC-2511 (Figure S23). The L10K-10- and B5K-10-coated substrates were placed in the 12-well plate and incubated for 24 h. The number of cells on the L10K-10- and B5K-10-coated substrate was significantly reduced, which indicated the antifouling properties. Moreover, the cell viability of the cells cultured with the polyether-coated substrate was similar to that of positive control, suggesting the biocompatibility of the catechol-functionalized polymer coatings.

The antifouling properties of the catechol-functionalized polymers were also demonstrated by a cell attachment test using another type of fibroblast cell, L929. While the cells showed normal adhesion and proliferation on uncoated and PEG-treated glass surfaces (Figure S24), most cells deposited on the catechol-functionalized triblock copolymer-coated surface were found to be small and easily removed by washing, which demonstrated that the catechol-functionalized polymer effectively inhibited the adhesion of cells through surface hydration.

https://dx.doi.org/10.1021/acs.macromol.0c00481
Macromolecules XXXX, XXX, XXX−XXX

CONCLUSIONS

In summary, catechol-functionalized block copolymers were prepared to assess the effects of the composition and conformation on their antifouling properties. The bioinspired block copolymer exhibited surface-independent binding to both hydrophilic and hydrophobic surfaces, and its antifouling effect was evaluated by QCM and SFA using BSA as a model protein. The effect of composition was evaluated by varying the length of the PEG block and catechol block, which offers tunable surface grafting and a diminished trade-off between surface adhesion and protein adsorption. Regarding the geometrical conformation, the triblock loop polymers present strong steric repulsion and improved antifouling effects compared to those of the corresponding diblock brush copolymers. Detailed atomistic MD simulations revealed the underlying molecular features responsible for the superior antifouling properties of the loop polymer. This molecular information can be useful in further developing advanced antifouling polymeric materials in practical settings. Furthermore, the catechol-functionalized polymer inhibits cell attachment, which demonstrates its significant potential for biomedical applications.

ASSOCIATED CONTENT

Supporting Information

The Supporting Information is available free of charge at https://pubs.acs.org/doi/10.1021/acs.macromol.0c00481.

Synthetic protocols, detailed ^{1}H and ^{13}C NMR spectra, and ESI-MS of the monomer; ^{1}H NMR spectra, SEC, TGA, AND DSC data of polymers prepared; AFM images, contact angle, SFA, QCM-D, Raman, and cellular viability assay of polymer surface coating; and additional MD simulation data (PDF)

Brush polymer (B10K-10) (AVI)

Loop polymer (L10K-10) (AVI)

AUTHOR INFORMATION

Corresponding Authors

Chunggi Baig − *School of Energy and Chemical Engineering, Ulsan National Institute of Science and Technology (UNIST), Ulsan 44919, Republic of Korea;* orcid.org/0000-0001-8278-8804; Email: cbaig@unist.ac.kr

Dong Woog Lee − *School of Energy and Chemical Engineering, Ulsan National Institute of Science and Technology (UNIST), Ulsan 44919, Republic of Korea;* orcid.org/0000-0002-1572-9270; Email: dongwoog.lee@unist.ac.kr

Byeong-Su Kim − *Department of Chemistry, Yonsei University, Seoul 03722, Republic of Korea;* orcid.org/0000-0002-6419-3054; Email: bskim19@yonsei.ac.kr

Authors

Eeseul Shin − *Department of Chemistry, Yonsei University, Seoul 03722, Republic of Korea*

Chanoong Lim − *School of Energy and Chemical Engineering, Ulsan National Institute of Science and Technology (UNIST), Ulsan 44919, Republic of Korea;* orcid.org/0000-0001-6903-0855

Uk Jung Kang − *School of Energy and Chemical Engineering, Ulsan National Institute of Science and Technology (UNIST), Ulsan 44919, Republic of Korea*

Minseong Kim − *Department of Chemistry, Yonsei University, Seoul 03722, Republic of Korea; Department of Chemistry, Ulsan National Institute of Science and Technology (UNIST), Ulsan 44919, Republic of Korea;* orcid.org/0000-0002-2612-922X

Jinwoo Park − *School of Energy and Chemical Engineering, Ulsan National Institute of Science and Technology (UNIST), Ulsan 44919, Republic of Korea;* orcid.org/0000-0003-2921-2923

Dongseok Kim − *Department of Chemistry, Yonsei University, Seoul 03722, Republic of Korea*

Woojin Choi − *Department of Chemical & Biomolecular Engineering, Yonsei University, Seoul 03722, Republic of Korea*

Jinkee Hong − *Department of Chemical & Biomolecular Engineering, Yonsei University, Seoul 03722, Republic of Korea;* orcid.org/0000-0003-3243-8536

Complete contact information is available at: https://pubs.acs.org/10.1021/acs.macromol.0c00481

Author Contributions

$^{\perp}$E.S., C.L., and U.J.K. contributed equally to this work.

Notes

The authors declare no competing financial interest.

ACKNOWLEDGMENTS

This work was supported by the Samsung Research Foundation (SRFC-MA1602-07). We thank Prof. Sebyung Kang at UNIST for providing QCM-D equipment.

REFERENCES

(1) Bixler, G. D.; Bhushan, B. Biofouling: Lessons from Nature. *Philos. Trans. R. Soc., A* **2012**, *370*, 2381−2417.

(2) Davidson, I.; Scianni, C.; Hewitt, C.; Everett, R.; Holm, E.; Tamburri, M.; Ruiz, G. Mini-Review: Assessing the Drivers of Ship Biofouling Management − Aligning Industry and Biosecurity Goals. *Biofouling* **2016**, *32*, 411−428.

(3) Dalsin, J. L.; Hu, B.-H.; Lee, B. P.; Messersmith, P. B. Mussel Adhesive Protein Mimetic Polymers for the Preparation of Non-fouling Surfaces. *J. Am. Chem. Soc.* **2003**, *125*, 4253−4258.

(4) Viegas, T. X.; Bentley, M. D.; Harris, J. M.; Fang, Z.; Yoon, K.; Dizman, B.; Weimer, R.; Mero, A.; Pasut, G.; Veronese, F. M. Polyoxazoline: Chemistry, Properties, and Applications in Drug Delivery. *Bioconjugate Chem.* **2011**, *22*, 976−986.

(5) Tanaka, M.; Mochizuki, A.; Ishii, N.; Motomura, T.; Hatakeyama, T. Study of Blood Compatibility with Poly(2-Methoxyethyl Acrylate). Relationship between Water Structure and Platelet Compatibility in Poly(2-Methoxyethylacrylate-Co-2-Hydroxyethylmethacrylate). *Biomacromolecules* **2002**, *3*, 36−41.

(6) Mrabet, B.; Nguyen, M. N.; Majbri, A.; Mahouche, S.; Turmine, M.; Bakhrouf, A.; Chehimi, M. M. Anti-Fouling Poly(2-Hydoxyethyl Methacrylate) Surface Coatings with Specific Bacteria Recognition Capabilities. *Surf. Sci.* **2009**, *603*, 2422−2429.

(7) Liu, Q.; Singh, A.; Lalani, R.; Liu, L. Ultralow Fouling Polyacrylamide on Gold Surfaces via Surface-Initiated Atom Transfer Radical Polymerization. *Biomacromolecules* **2012**, *13*, 1086−1092.

(8) Fruijtier-Pölloth, C. Safety Assessment on Polyethylene Glycols (PEGs) and Their Derivatives as Used in Cosmetic Products. *Toxicology* **2005**, *214*, 1−38.

(9) Fahrländer, E.; Schelhaas, S.; Jacobs, A. H.; Langer, K. PEGylated Human Serum Albumin (HSA) Nanoparticles: Preparation, Characterization and Quantification of the PEGylation Extent. *Nanotechnology* **2015**, *26*, 145103.

(10) Prime, K. L.; Whitesides, G. M. Adsorption of Proteins onto Surfaces Containing End-Attached Oligo(Ethylene Oxide): A Model System Using Self-Assembled Monolayers. *J. Am. Chem. Soc.* **1993**, *115*, 10714−10721.

(11) Chen, J.; Wang, J.; Qi, P.; Li, X.; Ma, B.; Chen, Z.; Li, Q.; Zhao, Y.; Xiong, K.; Maitz, M. F.; et al. Biocompatibility Studies of Poly(Ethylene Glycol)-Modified Titanium for Cardiovascular Devices. *J. Bioact. Compat Polym.* **2012**, *27*, 565−584.
(12) Lee, B. P.; Messersmith, P. B.; Israelachvili, J. N.; Waite, J. H. Mussel-Inspired Adhesives and Coatings. *Annu. Rev. Mater. Res.* **2011**, *41*, 99−132.
(13) Sedó, J.; Saiz-Poseu, J.; Busqué, F.; Ruiz-Molina, D. Catechol-Based Biomimetic Functional Materials. *Adv. Mater.* **2013**, *25*, 653−701.
(14) Wei, Q.; Achazi, K.; Liebe, H.; Schulz, A.; Noeske, P.-L. M.; Grunwald, I.; Haag, R. Mussel-Inspired Dendritic Polymers as Universal Multifunctional Coatings. *Angew. Chem., Int. Ed.* **2014**, *53*, 11650−11655.
(15) Ryu, J. H.; Lee, Y.; Kong, W. H.; Kim, T. G.; Park, T. G.; Lee, H. Catechol-Functionalized Chitosan/Pluronic Hydrogels for Tissue Adhesives and Hemostatic Materials. *Biomacromolecules* **2011**, *12*, 2653−2659.
(16) Shin, E.; Ju, S. W.; An, L.; Ahn, E.; Ahn, J.-S.; Kim, B.-S.; Ahn, B. K. Bioinspired Catecholic Primers for Rigid and Ductile Dental Resin Composites. *ACS Appl. Mater. Interfaces* **2018**, *10*, 1520−1527.
(17) Seo, S.; Lee, D. W.; Ahn, J. S.; Cunha, K.; Filippidi, E.; Ju, S. W.; Shin, E.; Kim, B.-S.; Levine, Z. A.; Lins, R. D.; Israelachvili, J. N.; Waite, J. H.; Valentine, M. T.; Shea, J. E.; Ahn, B. K. Significant Performance Enhancement of Polymer Resins by Bioinspired Dynamic Bonding. *Adv. Mater.* **2017**, *29*, 1703026.
(18) Thomas, A.; Bauer, H.; Schilmann, A.-M.; Fischer, K.; Tremel, W.; Frey, H. The "Needle in the Haystack" Makes the Difference: Linear and Hyperbranched Polyglycerols with a Single Catechol Moiety for Metal Oxide Nanoparticle Coating. *Macromolecules* **2014**, *47*, 4557−4566.
(19) Chaicham, A.; Sahasithiwat, S.; Tuntulani, T.; Tomapatanaget, B. Highly Effective Discrimination of Catecholamine Derivatives via FRET-on/off Processes Induced by the Intermolecular Assembly with Two Fluorescence Sensors. *Chem. Commun.* **2013**, *49*, 9287−9289.
(20) Liu, S.; Chen, L.; Tan, L.; Cao, F.; Bai, L.; Wang, Y. A High Efficiency Approach for a Titanium Surface Antifouling Modification: PEG-o-Quinone Linked with Titanium via Electron Transfer Process. *J. Mater. Chem. B* **2014**, *2*, 6758−6766.
(21) Kim, H. S.; Ham, H. O.; Son, Y. J.; Messersmith, P. B.; Yoo, H. S. Electrospun Catechol-Modified Poly(Ethyleneglycol) Nanofibrous Mesh for Anti-Fouling Properties. *J. Mater. Chem. B* **2013**, *1*, 3940−3949.
(22) Kang, T.; Banquy, X.; Heo, J.; Lim, C.; Lynd, N. A.; Lundberg, P.; Oh, D. X.; Lee, H.-K.; Hong, Y.-K.; Hwang, D. S.; Waite, J. H.; Israelachvili, J. N.; Hawker, C. J. Mussel-Inspired Anchoring of Polymer Loops That Provide Superior Surface Lubrication and Antifouling Properties. *ACS Nano* **2016**, *10*, 930−937.
(23) Lee, H.; Lee, K. D.; Pyo, K. B.; Park, S. Y.; Lee, H. Catechol-Grafted Poly(Ethylene Glycol) for PEGylation on Versatile Substrates. *Langmuir* **2010**, *26*, 3790−3793.
(24) Patil, N.; Falentin-Daudré, C.; Jérôme, C.; Detrembleur, C. Mussel-Inspired Protein-Repelling Ambivalent Block Copolymers: Controlled Synthesis and Characterization. *Polym. Chem.* **2015**, *6*, 2919−2933.
(25) Duan, J.; Wu, W.; Wei, Z.; Zhu, D.; Tu, H.; Zhang, A. Synthesis of Functional Catechols as Monomers of Mussel-Inspired Biomimetic Polymers. *Green Chem.* **2018**, *20*, 912−920.
(26) Divandari, M.; Morgese, G.; Trachsel, L.; Romio, M.; Dehghani, E. S.; Rosenboom, J.-G.; Paradisi, C.; Zenobi-Wong, M.; Ramakrishna, S. N.; Benetti, E. M. Topology Effects on the Structural and Physicochemical Properties of Polymer Brushes. *Macromolecules* **2017**, *50*, 7760−7769.
(27) Greene, G. W.; Martin, L. L.; Tabor, R. F.; Michalczyk, A.; Ackland, L. M.; Horn, R. Lubricin: A Versatile, Biological Anti-Adhesive with Properties Comparable to Polyethylene Glycol. *Biomaterials* **2015**, *53*, 127−136.
(28) Waller, K. A.; Zhang, L. X.; Elsaid, K. A.; Fleming, B. C.; Warman, M. L.; Jay, G. D. Role of Lubricin and Boundary Lubrication in the Prevention of Chondrocyte Apoptosis. *Proc. Natl. Acad. Sci. U.S.A.* **2013**, *110*, 5852−5857.
(29) Morgese, G.; Trachsel, L.; Romio, M.; Divandari, M.; Ramakrishna, S. N.; Benetti, E. M. Topological Polymer Chemistry Enters Surface Science: Linear versus Cyclic Polymer Brushes. *Angew. Chem., Int. Ed.* **2016**, *55*, 15583−15588.
(30) Dalsin, J. L.; Lin, L.; Tosatti, S.; Vörös, J.; Textor, M.; Messersmith, P. B. Protein Resistance of Titanium Oxide Surfaces Modified by Biologically Inspired MPEG-DOPA. *Langmuir* **2005**, *21*, 640−646.
(31) Niederer, K.; Schüll, C.; Leibig, D.; Johann, T.; Frey, H. Catechol Acetonide Glycidyl Ether (CAGE): A Functional Epoxide Monomer for Linear and Hyperbranched Multi-Catechol Functional Polyether Architectures. *Macromolecules* **2016**, *49*, 1655−1665.
(32) Shin, E. Mussel-Inspired Polyglycerol: Synthesis and Versatile Surface Modification. M.Sc. Thesis, Ulsan National Institute of Science & Technology, 2015.
(33) Misaka, H.; Tamura, E.; Makiguchi, K.; Kamoshida, K.; Sakai, R.; Satoh, T.; Kakuchi, T. Synthesis of End-Functionalized Polyethers by Phosphazene Base-Catalyzed Ring-Opening Polymerization of 1,2-Butylene Oxide and Glycidyl Ether. *J. Polym. Sci., Part A: Polym. Chem.* **2012**, *50*, 1941−1952.
(34) Israelachvili, J.; Min, Y.; Akbulut, M.; Alig, A.; Carver, G.; Greene, W.; Kristiansen, K.; Meyer, E.; Pesika, N.; Rosenberg, K.; et al. Recent Advances in the Surface Forces Apparatus (SFA) Technique. *Rep. Prog. Phys.* **2010**, *73*, 036601.
(35) Yoo, J.; Birke, A.; Kim, J.; Jang, Y.; Song, S. Y.; Ryu, S.; Kim, B.-S.; Kim, B.-G.; Barz, M.; Char, K. Cooperative Catechol-Functionalized Polypept(o)Ide Brushes and Ag Nanoparticles for Combination of Protein Resistance and Antimicrobial Activity on Metal Oxide Surfaces. *Biomacromolecules* **2018**, *19*, 1602−1613.
(36) Al-Shakhshir, R. H.; Regnier, F. E.; White, J. L.; Hem, S. L. Contribution of Electrostatic and Hydrophobic Interactions to the Adsorption of Proteins by Aluminium-Containing Adjuvants. *Vaccine* **1995**, *13*, 41−44.
(37) Yang, Z.; Galloway, J. A.; Yu, H. Protein Interactions with Poly(Ethylene Glycol) Self-Assembled Monolayers on Glass Substrates: Diffusion and Adsorption. *Langmuir* **1999**, *15*, 8405−8411.
(38) Sheth, S. R.; Leckband, D. Measurements of Attractive Forces between Proteins and End-Grafted Poly(Ethylene Glycol) Chains. *Proc. Natl. Acad. Sci. U.S.A.* **1997**, *94*, 8399−8404.
(39) Bosker, W. T. E.; Iakovlev, P. A.; Norde, W.; Cohen Stuart, M. A. BSA Adsorption on Bimodal PEO Brushes. *J. Colloid Interface Sci.* **2005**, *286*, 496−503.
(40) Li, L.; Yan, B.; Zhang, L.; Tian, Y.; Zeng, H. Mussel-inspired antifouling coatings bearing polymer loops. *Chem. Commun.* **2015**, *51*, 15780−15783.
(41) Wang, X.; Berger, R.; Ramos, J. I.; Wang, T.; Koynov, K.; Liu, G.; Butt, H.-J.; Wu, S. Nanopatterns of polymer brushes for understanding protein adsorption on the nanoscale. *RSC Adv.* **2014**, *4*, 45059−45064.
(42) De Vos, W. M.; Biesheuvel, P. M.; De Keizer, A.; Kleijn, J. M.; Stuart, M. A. C. Adsorption of the protein bovine serum albumin in a planar poly(acrylic acid) brush layer as measured by optical reflectometry. *Langmuir* **2008**, *24*, 6585−6584.
(43) Benetti, E. M.; Divandari, M.; Ramakrishna, S. N.; Morgese, G.; Yan, W.; Trachsel, L. Loops and Cycles at Surfaces: The Unique Properties of Topological Polymer Brushes. *Chem.-Eur J.* **2017**, *23*, 12433−12442.
(44) Choi, W.; Jin, J.; Park, S.; Kim, J.-Y.; Lee, M.-J.; Sun, H.; Kwon, J.-S.; Lee, H.; Choi, S.-H.; Hong, J. Quantitative Interpretation of Hydration Dynamics Enabled the Fabrication of Zwitterionic Antifouling Surface. *ACS Appl. Mater. Interfaces* **2020**, *12*, 7951−7965.
(45) Lüsse, S.; Arnold, K. The interaction of poly(ethylene glycol) with water studied by ^{1}H and ^{2}H NMR relaxation time measurements. *Macromolecules* **1996**, *29*, 4251−4257.
(46) Kim, J. M.; Baig, C. Precise Analysis of Polymer Rotational Dynamics. *Sci. Rep.* **2016**, *6*, 19127.

https://dx.doi.org/10.1021/acs.macromol.0c00481
Macromolecules XXXX, XXX, XXX−XXX

(47) Israelachvili, J. N. Thin Film Studies Using Multiple-Beam Interferometry. *J. Colloid Interface Sci.* **1973**, *44*, 259−272.
(48) Lowrey, D. D.; Tasaka, K.; Kindt, J. H.; Banquy, X.; Belman, N.; Min, Y.; Pesika, N. S.; Mordukhovich, G.; Israelachvili, J. N. High-Speed Friction Measurements Using a Modified Surface Forces Apparatus. *Tribol. Lett.* **2011**, *42*, 117−127.
(49) Huang, X.; Bai, Q.; Hu, J.; Hou, D. A Practical Model of Quartz Crystal Microbalance in Actual Applications. *Sensors* **2017**, *17*, 1785.
(50) Hu, Q.; Ouyang, S.; Li, J.; Cao, Z. Raman spectroscopic investigation on pure D_2O/H_2O from 303 to 573 K: interpretation and implications for water structure. *J. Raman Spectrosc.* **2017**, *48*, 610−617.
(51) Phillips, J. C.; Braun, R.; Wang, W.; Gumbart, J.; Tajkhorshid, E.; Villa, E.; Chipot, C.; Skeel, R. D.; Kalé, L.; Schulten, K. Scalable Molecular Dynamics with NAMD. *J. Comput. Chem.* **2005**, *26*, 1781−1802.
(52) Vanommeslaeghe, K.; Hatcher, E.; Acharya, C.; Kundu, S.; Zhong, S.; Shim, J.; Darian, E.; Guvench, O.; Lopes, P.; Vorobyov, I.; et al. CHARMM General Force Field: A Force Field for Drug-like Molecules Compatible with the CHARMM All-Atom Additive Biological Force Fields. *J. Comput. Chem.* **2010**, *31*, 671−690.
(53) Dassault Systèmes BIOVIA. *Materials Studio, 6.1*; Dassault Systèmes: San Diego, 2014.
(54) Jorgensen, W. L.; Chandrasekhar, J.; Madura, J. D.; Impey, R. W.; Klein, M. L. Comparison of Simple Potential Functions for Simulating Liquid Water. *J. Chem. Phys.* **1983**, *79*, 926−935.
(55) Humphrey, W.; Dalke, A.; Schulten, K. VMD - Visual Molecular Dynamics. *J. Mol. Graph. Model.* **1996**, *14*, 33−38.
(56) Darden, T.; York, D.; Pedersen, L. Particle Mesh Ewald: An N·log(N) Method for Ewald Sums in Large Systems. *J. Chem. Phys.* **1993**, *98*, 10089.
(57) Hardy, D. J.; Wu, Z.; Phillips, J. C.; Stone, J. E.; Skeel, R. D.; Schulten, K. Multilevel Summation Method for Electrostatic Force Evaluation. *J. Chem. Theory Comput.* **2015**, *11*, 766−779.

https://dx.doi.org/10.1021/acs.macromol.0c00481
Macromolecules XXXX, XXX, XXX−XXX